

# DiffSRL: Learning Dynamic-aware State Representation for Deformable Object Control with Differentiable Simulation

Sirui Chen\*, Yunhao Liu\*, Jialong Li, Shang Wen Yao, Tingxiang Fan, Jia Pan<sup>†</sup>

**Abstract**—Dynamic state representation learning is an important task in robot learning. Latent space that can capture dynamics related information has wide application in areas such as accelerating model free reinforcement learning, closing the simulation to reality gap, as well as reducing the motion planning complexity. However, current dynamic state representation learning methods scale poorly on complex dynamic systems such as deformable objects, and cannot directly embed well defined simulation function into the training pipeline. We propose DiffSRL, a dynamic state representation learning pipeline utilizing differentiable simulation that can embed complex dynamics models as part of the end-to-end training. We also integrate differentiable dynamic constraints as part of the pipeline which provide incentives for the latent state to be aware of dynamical constraints. We further establish a state representation learning benchmark on a soft-body simulation system, PlasticineLab, and our model demonstrates superior performance in terms of capturing long-term dynamics as well as reward prediction. The source code and more experiments results is available at <https://ericccsr.github.io/DiffSRL/>.

## I. INTRODUCTION

Deep neural networks have become a powerful tool in representing high dimensional data using fewer dimensions. Its rapid development and application nowadays have significantly enhanced and accelerated the machines to process complex data such as images, words, sentences, and graphs. Among the applications, one that has recently aroused great research interest is representing real-world objects in dynamical environments from high dimensional point clouds or images for control. Low dimension latent state can benefit learning algorithms by reducing the trainable parameters, accelerating the training, as well as achieving better control result. The efficiency of this paradigm on rigid-body objects has been demonstrated in recent research [1], [2].

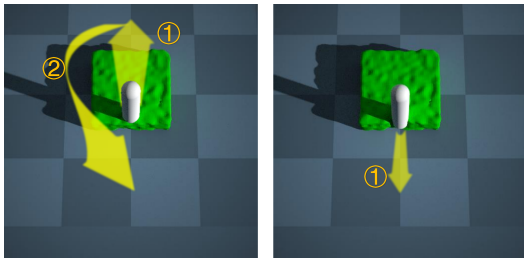


Fig. 1: Similar states but expecting distinct action trajectories.

However, representing more commonly seen deformable objects in low dimension remains to be a challenging problem [3] and is essential for deformable object manipulation.

Representing deformable objects is difficult for multiple reasons: a) The state of objects tends to be extremely large due to their high degrees of freedom (DoFs) during deformation [3]. For example, a piece of cloth can be translated integrally like an ordinary rigid object. But it can also be rolled, crumpled, and folded with no predetermined pattern. Due to the complexity resulting from high DoFs, soft-body objects lack uniform and convenient representations but rely on surface particles or meshes to record their current states. b) Different state elements of the same deformable object can have very different correlations when undergoing different deformation [3]. For instance, surface points on a piece of unfolded cloth, when being translated forward, all obey the same movement. However, once being folded, the cloth divides into upper and lower parts where surface points move in opposite directions. c) Visually similar states can generate distinct outcomes, which can confuse most static state representation learning methods. Fig. 1 shows one such example where a robotic arm is removing a rod from a piece of plasticine and then placing it at a target position. The initial states of the given two situations are similar but with subtle differences: on the left, the rod is completely surrounded by plasticine while on the right there is a large enough notch in the plasticine. The difference between them can be overlooked by static representation learning approaches because the notch occupies merely a tiny number of volume. As a result, the controller will generate resemblant actions while we prefer the robotic arm to first drag the rod out (action ①) and then translate it (action ②) in the first case, and a direct translation towards the target is more desirable for the second one. Similar challenges are ubiquitous in soft-body object manipulation, calling for the development of new state representation learning algorithms that are dynamic-aware, i.e., the representation shall not only examine the current state but also understand the dynamics to reflect different futures bifurcated from similar current states.

Existing state representation learning methods, such as AutoEncoder [2] and Embed to Control (E2C) [1], lack specific designs for dealing with the above challenges brought by the dynamics of deformable objects. Newly emerged solutions focusing on deformable objects, such as CFM [3] or G-Doom [4], as will be elaborated in Sec. II, cannot directly embed simulation into their training pipelines, leading to the performance bottleneck on soft-body object manipulation tasks [5]. To improve the performance of state representation learning on deformable objects, we hereby propose a new pipeline DiffSRL that utilizes a differentiable simulator to better encode dynamic- and constraint-aware information.

\* denotes equal contribution. <sup>†</sup> denotes the corresponding author.

S. Chen, Y. Liu, J. Li, S. Yao, T. Fan, J. Pan are with the University of Hong Kong.

Our main contributions are threefold.

- We propose an end-to-end dynamic state representation learning pipeline utilizing differentiable simulation to capture multistep dynamic of deformable objects. To the best of our knowledge, this is the first time that state representation learning directly uses the ground truth simulation function as part of the end-to-end training pipeline.
- Our method explicitly considers dynamics constraints related to the training pipeline and demonstrates awareness of physical constraints.
- We establish a benchmark on PlasticineLab [6], a non-Newtonian deformable object simulation environment. As baselines, we also implement a set of state-of-the-art state representation learning algorithms, such as CFM [3], inverse model learning [7], AutoEncoder [2] and E2C [1].

We have compared our proposed pipeline and baselines according to the reward prediction accuracy and the trajectory reconstruction errors, and investigated the performance of the learned encoder on important downstream tasks such as model-free reinforcement learning and model-based policy optimization. We have demonstrated that our approach outperforms all baselines on all tasks most of the time.

## II. RELATED WORK

Dynamic state representation learning is an emerging topic together with reinforcement learning for the acceleration and enhancement it offers. Auto-Encoder [2] trains a CNN encoder-decoder pair to extract features from images to achieve better performances in deep reinforcement learning than training all parameters from scratch. This method, however, only uses static state information and will fail to distinguish visually similar but dynamically different states [5] as previously shown. As a solution to this issue, Embed to Control (E2C) [1] proposes a pipeline including a learned forward model, an auto-encoder, and a linear dynamic transfer constraint between each current state and the next state. E2C demonstrates its strength in enhancing deep RL's performance in target-reaching problems with image observations, but its linear model cannot well describe the complex dynamics of deformable objects especially for multiple steps. Replacing the linear model in E2C with a neural network is not trivial because the neural net with significantly more parameters may be hard to converge and prevent the E2C variant from achieving desirable outcomes as well as failed to rollout accurate long run trajectories. Alternatively, the Inverse-model based state representation learning [8] is based on the heuristics that good state representation should be able to predict action leading to the transfer between two consecutive states. Thus, the encoder can be trained with an action predictor by minimizing the MSE loss between real and predicted action. Inverse model based method has been further applied in model-free RL tasks [9], [10], with more variants and applications elucidated in [5], but existing designs do not take the complexity of deformable objects into consideration either. CFM [3] explored the

area of state representation learning on deformable objects such as clothes and ropes. It utilizes contrastive learning to jointly train both the forward model and the encoder to represent images of deformable objects with distinguishable latent states. The trained forward model and latent space has been used in some MPC-based manipulation control. G-Doom [4] applies a similar paradigm as CFM but with a different architecture in terms of using latent graphs as the representation in the latent space and graph dynamic models as the forward model. However, despite their achievement in manipulating deformable objects, both CFM and G-Doom assume no access to the ground-truth analytical model of the dynamic system and didn't take physical constraints into consideration, which may lead to their forward models' incapability in accurate long-term planning.

Recent advances of physically-based simulation, such as Material Point Method (MPM) [11], allow us to accurate and efficiently simulate deformable objects such as cloth and plasticine. What's more, the differentiable simulator [12]–[14] allows each simulation step to be integrated as a layer in deep neural networks, making end-to-end training possible. This provide opportunity to overcome the difficulty of capture complex dynamic with a neural net faced by E2C, CFM and G-DOOM. In end-to-end training, gradients from the upstream neural networks are propagated through physics engines and affect network parameters accordingly. For instance, DiffTaichi [14], a newly-emerged differentiable physics engine based on Taichi programming language [15], has included many MPM simulation examples and established a soft-body control benchmark with differentiable simulation in PlasticineLab [6]. We will also perform our experiments on PlasticineLab for a fair comparison among different methods.

As for the states to be encoded, common methods take 2D images as the input and thus adopt the convolution methods. But they may encounter difficulties when being applied in point clouds, due to the intrinsic permutation irregularity of point clouds. PointNet [16] is a pioneering work of applying deep learning on point cloud data, where the permutation invariance is achieved using point-wise symmetric functions, including point-wise MLP and max-pooling layers. Moreover, being trained on point clouds allows the deep learning algorithms to tolerate the variety of input shapes, regardless of how many points are contained in the incoming point clouds. Thus, our proposed DiffSRL method will utilize point clouds to extract samples from the PlasticineLab environment as the training dataset.

## III. PROBLEM FORMULATION

A general dynamic system consists of three components: a state space  $\mathcal{S}$ , an action space  $\mathcal{A}$ , and a transfer function:

$$s_{t+1} = f_{\text{sim}}(s_t, a_t), \quad s_t, s_{t+1} \in \mathcal{S}; a_t \in \mathcal{A}. \quad (1)$$

The state  $s_t$ , obtained from the differentiable simulator, is a mixture of observable parts (such as the particles' coordinates) and imperceptible parts (including the velocity fields and constraints). The observable part of the state

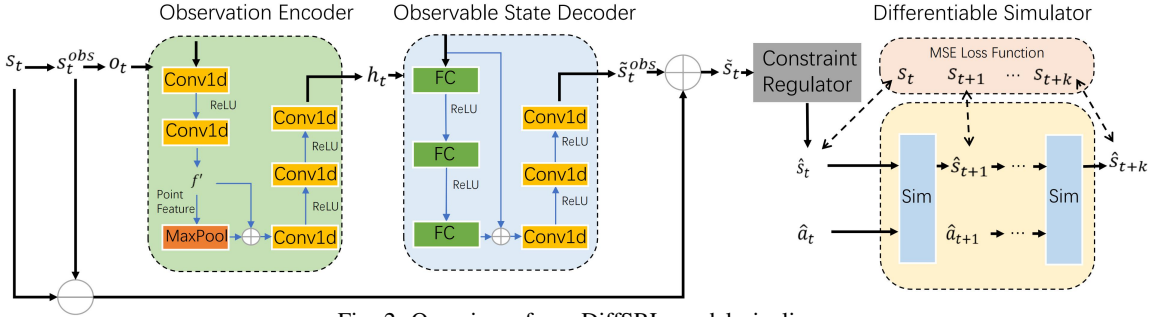


Fig. 2: Overview of our DiffSRL model pipeline.

$s_t$  is denoted as  $s_t^{\text{obs}}$ . The sensors of the robotic system may only observe part of the entire observable surroundings (denoted as  $\mathcal{O}$ ) due to its limited visual angles or occlusion of obstacles. This can be modeled as an observation function  $o_t = g_{\text{obs}}(s_t^{\text{obs}})$ , which selects accessible observation from observable states. Our goal is to establish a dynamic system state representation learning method capable of computing a low dimensional latent state  $h_t$  mapped from observation:  $h_t = f^\theta(o_t), o \in \mathcal{O}$ . The mapping function  $f^\theta$  is expected to capture sufficient information from the current state observation related to dynamics so that it can figure out whether two latent states are dynamically equivalent or not. In particular, two latent states  $h_t$  and  $h'_t$  are regarded as dynamically equivalent if given an arbitrary action sequence  $a_t, a_{t+1}, \dots, a_{t+k}$ , their future states  $s_{t+k}, s'_{t+k}$  will be similar.

#### IV. APPROACH

To learn the state representation that is aware of dynamic-equivalence, we propose the DiffSRL framework, which consists of three main components: 1) a state observation Autoencoder, which compresses the dynamic state to a latent state and reconstructs the state from latent state; 2) a constraint regulator, which regulates the decoded state against system dynamical constraints, and 3) a differentiable simulator, which rolls out the trajectory starting from the decoded state. The rolling-out process is differentiable so that gradients can be propagated from the end of the trajectory all the way back to the encoder. The overall pipeline of DiffSRL is shown in Fig. 2.

In this section, we will first introduce some preliminary knowledge of the Particle-In-Cell paradigm and the differentiability relevant to the simulator component in our design, and then move on to design details of the three major components of our model as well as our loss function.

##### A. Preliminaries

**Particle-In-Cell paradigm:** Lagrangian methods and Euler methods are two major branches of simulation algorithms [11]. The former method carries physical property with particles and is convenient for numerical integration; while the latter one stores physical properties on fixed grids and can be used for fast interactive simulation. The Particle-In-Cell (PIC) method is a combination of both methods and is commonly applied in fluid and deformable object simulation. The deformable object simulation in PlasticineLab is

based on Material Point Method [11], a variant of Particle-In-Cell. Our constraint regulator also utilizes PIC paradigm to efficiently detect penetration.

**Differentiable Simulation:** Physically-based simulation in Eq. (1) maps the current state  $s_t$  and action  $a_t$  to the next state  $s_{t+1}$ . Traditional simulators such as Bullet [17], Dart [18], Mujoco [19] only provide non-differentiable forward functions. Thanks to the recent advances in differentiable simulation Sec. II, now the gradient of simulation function can be also acquired:

$$\begin{aligned} \nabla s_t &= \nabla s_{t+1} \text{Jac}_{s_t}^{s_{t+1}} f(s_t, a_t) \\ \nabla a_t &= \nabla s_{t+1} \text{Jac}_{a_t}^{s_{t+1}} f(s_t, a_t) \end{aligned} \quad (2)$$

which allows us to embed the simulation function into a deep learning pipeline such as Pytorch and Tensorflow as part of the end-to-end training pipeline. In DiffSRL’s architecture, the trajectory rolling-out module is based on differentiable simulation.

**Distance Metric on Point Clouds:** Point clouds usually are expressed as an unordered set whose distance cannot be directly measured by common metrics such as MSE or MAE. Instead, here we use the Earth Mover’s Distance (EMD) [20] to measure the difference between two point clouds in terms of the minimum total pairwise distance between all the points. The EMD distance can be expressed as:

$$\text{Dist}_{\text{emd}}(A, B) = \min_{\phi: A \rightarrow B} \sum_{a \in A} d(a, \phi(a)) \quad (3)$$

where  $A$  and  $B$  are two unordered sets,  $d(\cdot, \cdot)$  is the distance between two points from these two sets, and  $\phi(\cdot)$  is the correspondence between  $a$  and  $b$  to be optimized. The minimization is implemented using Iterative Closest Point (ICP) [21] algorithm. Due to the high computational cost when solving this optimization, in practice, a greedy point matching based variant of EMD, Chamfer Distance [22], is also commonly used, which averages all the nearest neighbor distance by nearest neighbors:

$$\text{Dist}_{\text{chamfer}}(A, B) = \sum_{a \in A} \min_{b \in B} d(a, b) + \sum_{b \in B} \min_{a \in A} d(a, b). \quad (4)$$

We will use the losses based on Chamfer Distance and ICP algorithm as the constraint regulator.

##### B. State Observation Autoencoder

To obtain the latent states of a dynamic system, we use a deep neural network with learnable parameters  $\theta_{\text{encoder}}$  as the

encoder, where the specific architecture depends on the type of system’s observation. In particular, we will use Multi-layer Perceptron (MLP), Convolution Neural Network (CNN), and permutation invariant encoders such as PointNet [16] for observations in form of an ordered vector, image, or an unordered set of particles such as point clouds, respectively. Meanwhile, a decoder with parameters  $\theta_{\text{decoder}}$  is trained simultaneously for recovering the observable state from the latent state. Formally, the Autoencoder can be expressed as:

$$\begin{aligned} h_t &= f^{\theta_{\text{encoder}}}(o_t), \\ \tilde{s}_t^{\text{obs}} &= f^{\theta_{\text{decoder}}}(h_t), \end{aligned} \quad (5)$$

where  $o_t, s_t^{\text{obs}}, h_t$  are as defined in Sec. III and  $\tilde{s}_t^{\text{obs}}$  is the reconstructed observation from  $h_t$ .

### C. Differentiable Constraint Regulator

After the reconstructed observable state  $\tilde{s}_t^{\text{obs}}$  is obtained from the decoder, the reconstructed state  $\tilde{s}_t$  can be obtained by replacing observable part  $s_t^{\text{obs}}$  from  $s_t$  with  $\tilde{s}_t^{\text{obs}}$ . However, the reconstructed state may violate hard dynamics constraints, such as non-interpenetration constraints, joint limit constraints, as well as continuity constraints within continuous deformable objects. Constraint violation usually causes simulator failure or significant numerical errors. Hence, it is necessary to maintain the encoder’s awareness of the constraints from observation throughout the training procedure to enforce the gradient to be accurate and meaningful. Therefore, the constraints regulator is designed to find the feasible state closest to the generated state and, meanwhile, punish the Autoencoder for reconstructing unrealistic states. Formally, the reconstructed state, the constraint regulator loss, and the regulated state are computed as

$$\tilde{s}_t = s_t \ominus s_t^{\text{obs}} \oplus \tilde{s}_t^{\text{obs}}, \quad (6)$$

$$\mathcal{L}_{\text{constraint}} = \min_{s \in \mathcal{S}} \text{Dist}(s, \tilde{s}_t), \quad (7)$$

$$\hat{s}_t = \arg \min_{s \in \mathcal{S}} \text{Dist}(s, \tilde{s}_t), \quad (8)$$

where  $\ominus$  and  $\oplus$  represent removing and adding back the observable parts from and to the full state, respectively. For ordered state vectors, the distance  $\text{Dist}$  can be measured directly as the weighted MSE between the two vectors; as for unordered states such as point clouds, we use EMD as the distance metric.

### D. Differentiable Simulator and loss design

By using the reconstructed state, the simulation in Eq. (1) then becomes

$$\hat{s}_{t+1} = f_{\text{sim}}(\hat{s}_t, a_t) \quad (9)$$

where  $\hat{s}_t$  is reconstructed state after regulation, onto which  $f_{\text{sim}}$  executes the input action  $a_t$  in the simulation world and reaches the corresponding result state  $\hat{s}_{t+1}$ . When being applied to an trajectory of length  $k$ , we obtain a sequence:

$$\hat{s}_{t:t+k} = \text{DiffRollout}(\hat{s}_t, a_{t:t+k}) \quad (10)$$

where DiffRollout refers to the successive execution of the simulator, starting from  $\hat{s}_t$ , along the trajectory consisting of an action sequence  $a_t, a_{t+1}, \dots, a_{t+k}$ .

The model is trained with both the constraints violation loss  $\mathcal{L}_{\text{constraint}}$  (Eq. (7)) and the multi-step reconstruction loss  $\mathcal{L}_{\text{multi-step}}$  defined as

$$\mathcal{L}_{\text{multi-step}} = \sum_{i=1}^k \gamma \text{Dist}(s_{t+i}, \hat{s}_{t+i}), \quad (11)$$

which punishes the distance between each state  $s_{t+i}$  in the ground truth trajectory and its correspondence in the rolling-out trajectory starting from the reconstructed state. A decaying factor  $\gamma$  is used to mitigate the gradient instability effect when performing back propagation through a long horizon. In this way, the total loss to be optimized is

$$\mathcal{L}_{\text{total}} = (1 - \beta) \mathcal{L}_{\text{multi-step}} + \beta \mathcal{L}_{\text{constraints}} \quad (12)$$

where the weight factor  $\beta$  is introduced to trade off among different terms through the entire training scheme. Initially, the state reconstructed by the decoder violates constraints significantly, so  $\beta$  is set to 1 to encourage the Autoencoder to respect the constraints in the physics system. Progressively,  $\beta$  decays exponentially at rate  $\lambda$  so that the multi-step reconstruction loss dominates.

## V. EXPERIMENTS AND RESULTS

To evaluate effectiveness of DiffSRL, we evaluated our model with three experiments: 1) trajectory reconstruction, 2) reward prediction, and 3) model-free reinforcement learning on *Chopsticks* and *Rope* tasks from the PlasticineLab benchmark [6]. Our proposed DiffSRL has achieved state-of-the-art performance in these experiments most of the time.

### A. Baselines for Comparison

We compared our approach against state-of-the-art method CFM [3] and four commonly used dynamic state representation learning methods: *E2C* [1], *Forward* [23] that learns a dynamic forward model on latent states, *Inverse* [7] that conducts inverse model learning for action prediction, as well as *AutoEncoder* directly reconstructing the state [2]. In Tab. I, we summarize characteristics of different approaches.

In terms of details of baseline implementation, similar to our method, we use Chamfer Distance [22] as loss function to train autoencoder in the baseline. The forward model used in E2C and Forward  $f_{\text{fwd}}^{\theta}(h_t, a_t)$  is 3 layer MLP on latent space, the action predictor  $a_t^{\text{pred}} = f_{\text{inverse}}^{\phi}(h_t, h_{t+1})$  in inverse model [7] uses concatenation of two latent states as input and predicts the action with a 3 layer MLP. The contrastive loss in [3] uses the same formation and negative sample selection method as in the original paper. All MLPs mentioned here use 256 as the size of a hidden layer.

### B. Implementation Details

Since PlasticineLab is a deformable object simulator based on Material Point Method (MPM) [11], the particles used for simulation can be naturally considered as an unordered point cloud. For simplicity, we choose each observation  $o_t$  as the

	predictive dynamic model	predict action	observation reconstruction	multipstep information	physical constraints
DiffSRL (Our)	✓		✓	✓	✓
E2C [1]	✓		✓		
Forward [23]	✓				
Inverse [7]		✓			
CFM [3]	✓				
Autoencoder [2]			✓		

TABLE I: Comparison of different components used in different state representation learning pipelines.

position of all particles at time  $t$ . An observation, together with velocity and other particle wise properties, forms a full state  $s_t$ . A variant of PCN [24] is then used to implement the Autoencoder for the point cloud  $o_t$ , with the detailed architecture presented in Fig. 2.

As for the constraint regulator, the MPM simulation disallows penetration between particles and rigid bodies, and therefore requires smooth velocity fields within continuous materials. Hence, our regulator is constructed in two stages: 1) The signed distance field (SDF) algorithm with MPM is used to enforce non-penetration and detect collisions efficiently. For those particles  $p_{\text{collide}}$  resided inside rigid bodies, we resolve the collision by finding the minimum distance  $d_{p_{\text{collide}}}$  to exit the colliding object. For simplicity, it is assumed that each rigid-body object is a geometric primitive and has analytical collision detection routine, so that the minimum exit distance can be solved efficiently using a simple linear programming solver. The loss function for this objective is defined as the sum of all  $d_{p_{\text{collide}}}$ . 2) The Iterative Cloest Point (ICP) algorithm is applied to find the best pairwise matches between particles in ground truth observation and those in the reconstructed one where some particles have been translated outside rigid-body objects to avoid collisions. This step is necessary because the decoded observation  $\tilde{o}_t$  are expected to satisfy soft-body dynamic properties from  $s_t$  such as continuous velocity fields. After pairwise relationships are established by ICP, the velocity and smoothness constraints of each ground-true particle are exerted to the matched pairs. The details are described in Algorithm 1 and also illustrated in Fig. 3.

The distance between the regulated observation and the corresponding ground truth is the sum of pairwise squared

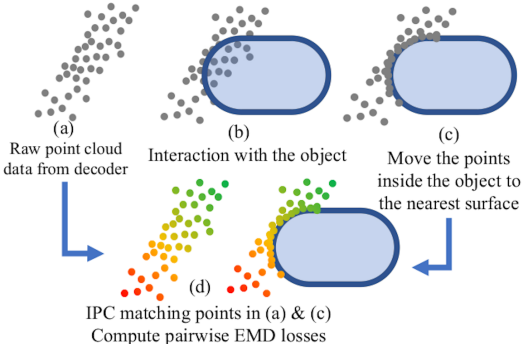


Fig. 3: Collision-free and smooth velocity field constraint regulator, where the dots and the capsule represent the point clouds and the rigid-body object which may collide with it, respectively.

## Algorithm 1 Constraints Regulator

```

Input: Rigid bodies  $\mathcal{R}$ , the ground-truth particle observable state  $s_t^{\text{obs}}$  (i.e., position of particles), and decoded particles position  $\tilde{s}_t^{\text{obs}}$ 
Initialize: Grids to store interpenetrating rigid bodies information  $c_{\text{grid}}^{\text{col}}$ , loss of penetration  $l_{\text{penetration}}$ , and loss reconstruction  $l_{\text{rec}}$ .
 $\hat{s}_t^{\text{obs, no-penetration}} \leftarrow \text{ResolvePenetration}(\mathcal{R}, \tilde{s}_t^{\text{obs}})$ 
     $\triangleleft$  Compute grid mass using particle-in-cell
 $m_{\text{grid}} \leftarrow \text{ComputeGridMass}(\hat{s}_t^{\text{obs}})$ 
for  $r$  in  $\mathcal{R}$  do
     $\triangleleft$  Check penetration using signed distance field
     $c_{\text{grid}}^{\text{col}} \leftarrow \text{SDF}(r, m_{\text{grid}})$ 
end for
     $\triangleleft$  Compute Interpenetration related information of each particle to all rigid bodies
for  $p$  in  $\hat{s}_t^{\text{obs no-penetration}}$  do
    if  $p.\text{grid}$  is not empty then
         $\triangleleft$  Solve linear programming problem to find minimum displacement for a particle to stay out of penetrating rigid body
         $p.\text{pos} \leftarrow \text{LPSolver}(\mathcal{R}, p)$ 
         $\triangleleft$  Sum up minimum displacement costs as loss
         $l_{\text{penetration}} += \text{LPCost}(r, p)$ 
    end if
end for
     $\triangleleft$   $\hat{s}_t^{\text{obs}} \leftarrow \text{ResolveSmoothness}(\hat{s}_t^{\text{obs no-penetration}})$ 
 $\text{order} \leftarrow \text{ICPSolver}(\hat{s}_t^{\text{obs}}, \hat{s}_t^{\text{obs}})$ 
 $\hat{s}_t^{\text{obs}} \leftarrow \text{perm}(\hat{s}_t^{\text{obs no-penetration}}, \text{perm}(\text{order}))$ 
return  $\hat{s}_t^{\text{obs}}$ 

```

distance, i.e., the EMD [20] distance between  $\tilde{o}_t$  and  $o_t$ .

### C. Data Collection

We collect 6,000 trajectories of length 8 from benchmarks *Chopsticks* and *Rope*. To make the datasets cover as many states as possible, 30% of data are sampled from random policies while others are collected when optimizing trajectories for manipulating different targets. This is because random actions frequently cause the manipulator to detach from the deformable object too early to capture sufficient deformation information. We use the ratio of 10:1:1 to split collected samples into training, validation and testing sets.

### D. Comparison in Trajectory Reconstruction

A straight forward evaluation of dynamical equivalence is the similarity between the real trajectory and the trajectory roll-out from the reconstructed state given the same action sequence, which is computed by accumulating the Chamfer Distance [22], i.e.,  $\sum_{s_{t:t+k}} D_{\text{chamfer}}(s_t, \hat{s}_t)$ , between each pairs of states in both trajectories. Some baseline methods such as *CFM*, *Forward* and *Inverse* only train the encoder without decoder and thus cannot reconstruct states. Thus, we trained a decoder for each fixed encoder using the Autoencoder training pipeline until convergence. Tab. II shows that DiffSRL achieves the best performance among all models.

Datasets	Rope		Chopsticks	
Metric	ChamferDist	MSE	ChamferDist	MSE
AutoEncoder	0.048	0.236	0.044	1.102
Inverse	0.042	0.276	0.048	1.19
Forward	0.083	5.435	0.124	6.599
E2C	0.048	<u>0.223</u>	0.064	1.244
CFM	<u>0.037</u>	0.236	0.037	<u>1.010</u>
DiffSRL	<b>0.027</b>	<b>0.218</b>	<b>0.031</b>	<b>0.840</b>
DiffSRL w/o Reg	0.039	0.292	<u>0.036</u>	1.226

TABLE II: Comparison of the average and standard deviation of trajectory rollout chamfer distance and mean squared error of reward prediction. The smaller the MSE and Chamfer Distance, the better the model. The best result is highlighted in **bold** and the second best is highlighted with underline. DiffSRL w/o Reg is our proposed method trained without non-penetration constraint regulator.

Moreover, to evaluate the effectiveness of the constraint regulator, we conduct an ablation study by removing non-penetration regulation modules during the training phase. It shows the removal of non-penetration regulator will result in higher trajectory reconstruction error as well as reward prediction error. We also tried to remove the smoothness regulator during training, but this will results in NaN in gradient from differentiable simulator since the MPM’s requirement that particles in the same grid have consistent properties can be violated. One thing worth noting is that the *Forward* model is the worst among all models, which may be because it tends to be trapped in a trivial minimum as mentioned in [5].

#### E. Comparison in Reward Prediction

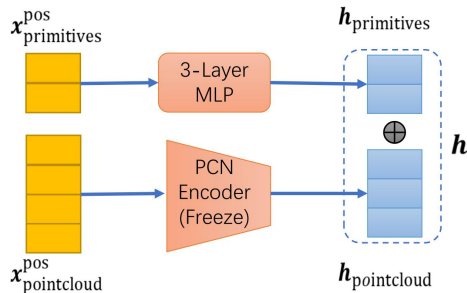


Fig. 4: The architecture of policy network that we used in model-based policy optimization and model-free reinforcement learning.

For many downstream control tasks, it is essential that the encoded latent states can capture the state’s main characters for accurate reward prediction. To predict rewards from latent states, we train a 3-layer MLP for latent states obtained from each encoder. The reward that is related to poses of the deformable object is the only part we predicted. The error is measured in mean square error:  $\frac{1}{|\mathcal{D}|} \sum_{s \in \mathcal{D}} \|\hat{r}_{\text{pred}} - r_{\text{real}}\|^2$ . As summarized in Tab. II, our model achieves the best performance on both datasets. The reward prediction error also increases when non-penetration regulator is absent.

#### F. Model-Based Policy Optimization (MBPO)

To investigate adaptability as well as effectiveness on various more complex downstream tasks, we first evaluated the encoders trained from different state representation

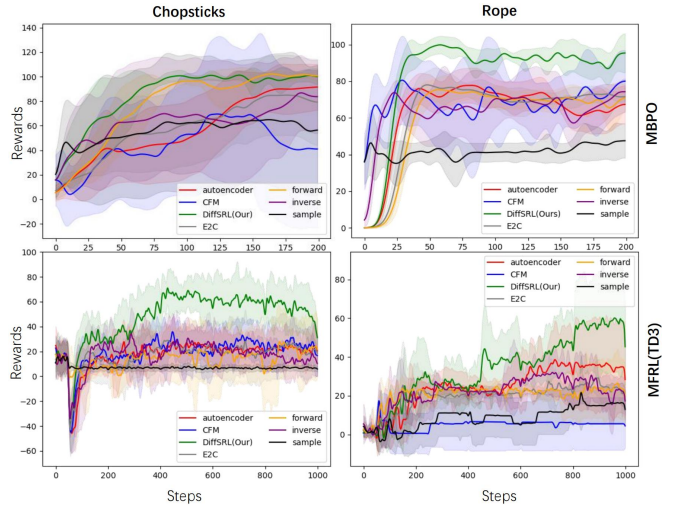


Fig. 5: TD3 Reward in different environments.

learning methods on end-to-end policy optimization with the differentiable simulator. Our experiment setting is similar to the end-to-end policy optimization in DiffTaichi [14], [25]. The trained policy is expected to control manipulators to move the plasticine to different target positions within finite steps. Detailed target and reward design are the same as described in [6]. The architecture of the policy network is shown in Fig. 4, where the encoder’s weights are fixed during policy optimization. For comparison, we add another baseline of the default down-sampling based method provided by PlasticineLab, which samples 400 points from each point cloud and keeps track of those points in the sampling order throughout the trajectory<sup>1</sup>. The policy network is initialized as a simple MLP and its inputs are obtained by concatenating features. We evaluated performance using the per-epoch average reward. Each experiment is repeated 5 times and the means and standard deviations are plotted in Fig. 5. The first row illustrates the reward of different methods in Chopstick and Rope environments, where most methods using state representation learning can improve their policies faster and achieve better final rewards, compared with the down-sampling based method. Moreover, our approach achieves the best result among all state representation learning methods including the *AutoEncoder* that is trained using a similar loss function. Surprisingly, the *Forward* method achieves competitive performance compared with other methods even though it has the worst performance in previous two tasks, which may indicate that the performance correlation between MBPO and reward / trajectory reconstruction is not significant and we will leave the study to the future work. Some key frames from the trajectory are shown in Fig. 6.

#### G. Model-Free Reinforcement Learning (MFRL)

Finally, we tested all models on model-free reinforcement learning on the same target-reaching tasks as described in MBPO. Since the trajectory information has been used in

<sup>1</sup>The down-sampling based method is not feasible in practice since tracking 400 points all the way on deformable object accurately is difficult.

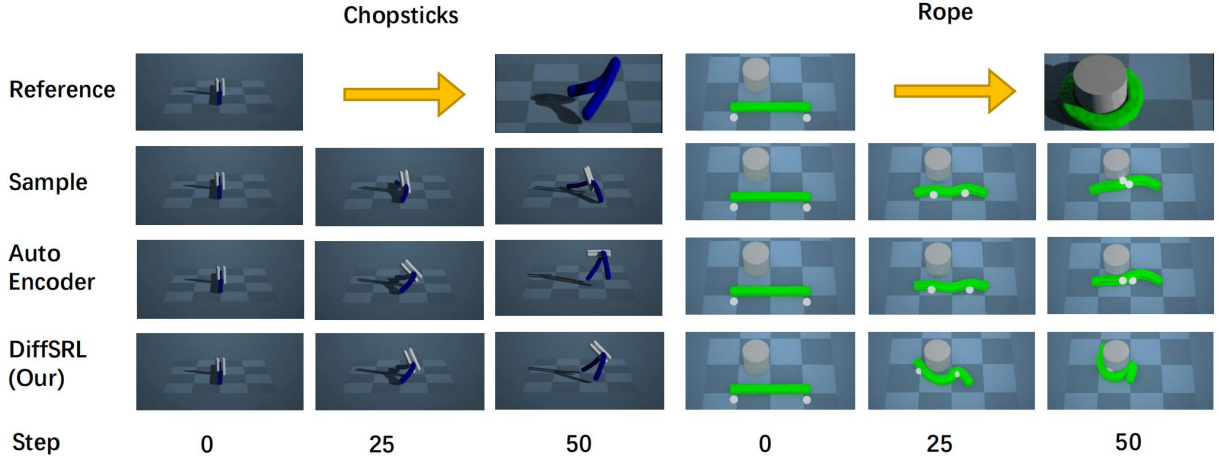


Fig. 6: Keyframes of different approaches in Model-Based Policy Optimization (MBPO) task.

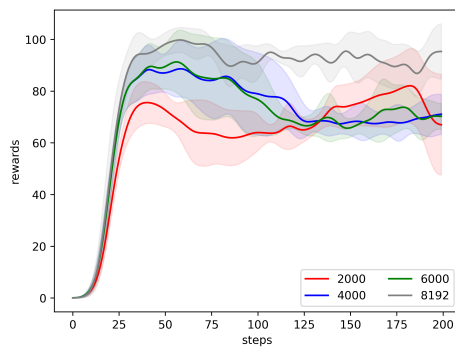


Fig. 7: Model based policy optimization reward in rope environment when using different number of point as encoder input.

MBPO experiments similar to on-policy reinforcement learning, to fully evaluate different state representation learning methods, our experiment uses the state-of-the-art off-policy algorithm TD3 [26], which uses latent state for both state value function and policy function. The architecture of policy function is shown in Fig. 4. We use similar experiments and evaluation criteria as MBPO but increase the epoch number from 200 to 1,000 since the model-free method requires more data. The results are shown in Fig. 5, from which we can observe that most state representation learning methods have higher maximum rewards and faster convergence speeds than the sample-based method, and DiffSRL achieves the best performance while CFM's performance in two environments are very different, implying its limitation in general situations.

#### H. Ablation Study

We conduct ablation study to show the effectiveness of constraints regulator. Since the removal of smoothness constraint regulator will crash the representation learning training procedure, we retrained the encoders using our pipeline without non-penetration constraints regulator and test them using MFRL and MBPO training to verify the effectiveness. Fig. 8 shows the result, we can justify the effectiveness of our design since the reward drop significantly if we remove the non-penetration regulator.

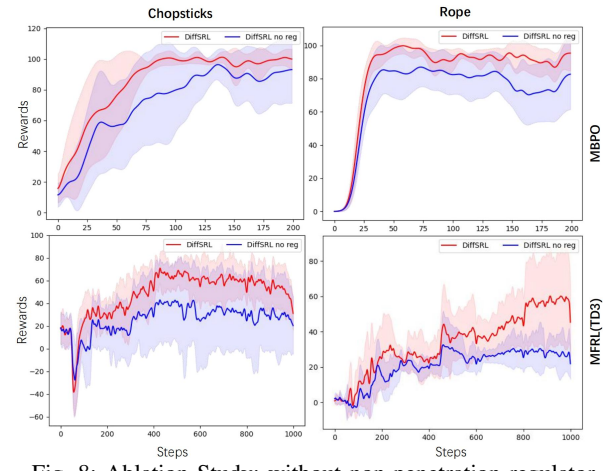


Fig. 8: Ablation Study: without non-penetration regulator

#### I. Robustness Analysis

The number of points observed by a sensor may vary greatly in real applications. Since the point cloud encoder can be directly applied on different point number without re-training, we use different numbers of observed points to test the robustness of our model. We trained a DiffSRL model using point clouds consisting of 8,192 points, and then investigated the deployment performance using 6,000, 4,000, 2,000 particles, by computing the reward curves when training MBPO from latent states. As shown in Fig. 7, although using fewer observable particles (from 8,192 to 6,000) than training will decrease the performance, further decreasing of the particle number (from 6,000 to 4,000 or 2,000) will not significantly downgrade the performance, which demonstrates that our method is relatively robust against disturbance in observation.

#### J. Hyperparameters Setting

Tab. III summarizes the hyperparameters used in our model. One important hyperparameter of our method is  $k$ , the number of trajectory rollout steps used when training the state representation. We choose  $k$  by evaluating the 10-step trajectory reconstruction loss on the validation set, with the result shown in Fig. 9. For both environments, 7-step

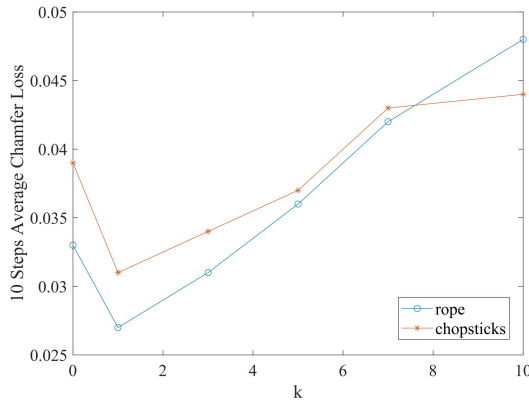


Fig. 9: 10-step Chamfer loss on both rope and chopstick benchmarks when using different number of training steps.

Parameters	Meaning	Value
N	Number of particles	8192
I	ICP iterations	3000
$d_{latent}$	Latent Space dimension	1024
$\alpha$	Learning rate	1e-5
$\gamma$	weight decay rate in 11	0.99
$\beta$	Initial weight between in 12	0.99
$\lambda$	Decay rate of $\beta$ per epoch	0.9
E	Number of epochs	20

TABLE III: Hyperparameters

achieves the best performance and thus we choose  $k = 7$ . Notice that the loss curve demonstrates non monotonic behavior as we increase the training step size, and the possible reason is that as the step size increases, the gradient back propagation though time tends to be more noisy due to numerical issues and the optimization landscape becomes more wiggly. We leave further investigation as future work.

## VI. CONCLUSION AND FUTURE WORK

We have presented a novel dynamic state representation learning model and its sample efficient training scheme. Moreover, we evaluated our model using multiple tasks on soft body benchmarks in PlasticineLab [6] and set up benchmarks to compare with other state-of-the-art models. Currently our model uses part of states directly from the simulator as observation, while in the real world, robots may not necessarily have sensors to access such information. In future, it is essential to extract the observation using physical sensors such as Lidar or cameras for deploying our method on real robots. One possible follow-up might include the differentiable rendering method [27] in our pipeline, which enables using easily accessible images as observation while maintaining the overall differentiability.

## REFERENCES

- [1] M. Watter, J. T. Springenberg, J. Boedecker, and M. A. Riedmiller, “Embed to control: A locally linear latent dynamics model for control from raw images,” in *NeurIPS*, 2015, pp. 2746–2754. [1](#), [2](#), [4](#), [5](#)
- [2] C. Finn, X. Y. Tan, Y. Duan, T. Darrell, S. Levine, and P. Abbeel, “Deep spatial autoencoders for visuomotor learning,” in *ICRA*, 2016, pp. 512–519. [1](#), [2](#), [4](#), [5](#)
- [3] W. Yan, A. Vangipuram, P. Abbeel, and L. Pinto, “Learning predictive representations for deformable objects using contrastive estimation,” *CoRR*, vol. abs/2003.05436, 2020. [1](#), [2](#), [4](#), [5](#)
- [4] X. Ma, D. Hsu, and W. S. Lee, “Learning latent graph dynamics for deformable object manipulation,” *CoRR*, vol. abs/2104.12149, 2021. [1](#), [2](#)
- [5] T. Lesort, N. D. Rodríguez, J. Goudou, and D. Filliat, “State representation learning for control: An overview,” *Neural Networks*, vol. 108, pp. 379–392, 2018. [1](#), [2](#), [6](#)
- [6] Z. Huang, Y. Hu, T. Du, S. Zhou, H. Su, J. B. Tenenbaum, and C. Gan, “Plasticinelab: A soft-body manipulation benchmark with differentiable physics,” in *ICLR*, 2021. [2](#), [4](#), [6](#), [8](#)
- [7] P. Agrawal, A. Nair, P. Abbeel, J. Malik, and S. Levine, “Learning to poke by poking: Experiential learning of intuitive physics,” *CoRR*, vol. abs/1606.07419, 2016. [2](#), [4](#), [5](#)
- [8] W. Duan and K. Jens, “Learning state representations for robotic control: Information disentangling and multi-modal learning,” Master’s thesis, TU Delft, 2017. [2](#)
- [9] E. Shelhamer, P. Mahmoudieh, M. Argus, and T. Darrell, “Loss is its own reward: Self-supervision for reinforcement learning,” in *ICLR*, 2017. [2](#)
- [10] D. Pathak, P. Agrawal, A. A. Efros, and T. Darrell, “Curiosity-driven exploration by self-supervised prediction,” in *CVPR Workshops*, 2017, pp. 488–489. [2](#)
- [11] C. Jiang, C. A. Schroeder, J. Teran, A. Stomakhin, and A. Selle, “The material point method for simulating continuum materials,” in *SIGGRAPH*, 2016, pp. 24:1–24:52. [2](#), [3](#), [4](#)
- [12] K. Werling, D. Omens, J. Lee, I. Exarchos, and C. K. Liu, “Fast and feature-complete differentiable physics engine for articulated rigid bodies with contact constraints,” in *RSS*, 2021. [2](#)
- [13] J. Xu, T. Chen, L. Zlokapa, M. Foshey, W. Matusik, S. Sueda, and P. Agrawal, “An end-to-end differentiable framework for contact-aware robot design,” in *RSS*, 2021. [2](#)
- [14] Y. Hu, L. Anderson, T. Li, Q. Sun, N. Carr, J. Ragan-Kelley, and F. Durand, “Difftaichi: Differentiable programming for physical simulation,” in *ICLR*, 2020. [2](#), [6](#)
- [15] Y. Hu, T. Li, L. Anderson, J. Ragan-Kelley, and F. Durand, “Taichi: a language for high-performance computation on spatially sparse data structures,” *ACM Trans. Graph.*, vol. 38, no. 6, pp. 201:1–201:16, 2019. [2](#)
- [16] C. R. Qi, H. Su, K. Mo, and L. J. Guibas, “Pointnet: Deep learning on point sets for 3d classification and segmentation,” in *CVPR*, 2017, pp. 77–85. [2](#), [4](#)
- [17] E. Coumans *et al.*, “Bullet physics library,” *Open source: bulletphysics.org*, vol. 15, no. 49, p. 5, 2013. [3](#)
- [18] J. Lee, M. X. Grey, S. Ha, T. Kunz, S. Jain, Y. Ye, S. S. Srinivasa, M. Stilman, and C. K. Liu, “DART: Dynamic animation and robotics toolkit,” *The Journal of Open Source Software*, vol. 3, no. 22, p. 500, 2018. [3](#)
- [19] E. Todorov, T. Erez, and Y. Tassa, “Mujoco: A physics engine for model-based control,” in *IROS*, 2012, pp. 5026–5033. [3](#)
- [20] Y. Rubner, C. Tomasi, and L. J. Guibas, “A metric for distributions with applications to image databases,” in *ICCV*, 1998, pp. 59–66. [3](#), [5](#)
- [21] K. S. Arun, T. S. Huang, and S. D. Blostein, “Least-squares fitting of two 3-d point sets,” *IEEE Trans. Pattern Anal. Mach. Intell.*, vol. 9, no. 5, pp. 698–700, 1987. [3](#)
- [22] M. Liu, O. Tuzel, A. Veeraraghavan, and R. Chellappa, “Fast directional chamfer matching,” in *CVPR*, 2010, pp. 1696–1703. [3](#), [4](#), [5](#)
- [23] L. Kaiser, M. Babaeizadeh, P. Milos, B. Osinski, R. H. Campbell, K. Czechowski, D. Erhan, C. Finn, P. Kozakowski, S. Levine, A. Mohiuddin, R. Sepassi, G. Tucker, and H. Michalewski, “Model based reinforcement learning for atari,” in *ICLR*, 2020. [4](#), [5](#)
- [24] W. Yuan, T. Khot, D. Held, C. Mertz, and M. Hebert, “PCN: point completion network,” in *3DV*, 2018, pp. 728–737. [5](#)
- [25] Y. Qiao, J. Liang, V. Koltun, and M. C. Lin, “Scalable differentiable physics for learning and control,” in *ICML*, vol. 119, 2020, pp. 7847–7856. [6](#)
- [26] S. Fujimoto, H. van Hoof, and D. Meger, “Addressing function approximation error in actor-critic methods,” in *ICML*, vol. 80, 2018, pp. 1582–1591. [7](#)
- [27] H. Kato, D. Beker, M. Morariu, T. Ando, T. Matsuoka, W. Kehl, and A. Gaidon, “Differentiable rendering: A survey,” *CoRR*, vol. abs/2006.12057, 2020. [8](#)